Contract No.:

This manuscript has been authored by Savannah River Nuclear Solutions (SRNS), LLC under Contract No. DE-AC09-08SR22470 with the U.S. Department of Energy (DOE) Office of Environmental Management (EM).

Examination of Climatological Wind Patterns and Simulated Pollen Dispersion in a Complex Island Environment

Brian J. Viner*, Raymond W. Arritt and Mark E. Westgate

B. J. Viner, Atmospheric Technologies Group, Savannah River National Laboratory, Aiken, SC 29808;

R. W. Arritt and M. E. Westgate, Department of Agronomy, Iowa State University, Ames, IA 50011.

*Corresponding author information:

Email: Brian.Viner@srnl.doe.gov

Phone: (803) 725-3318

Fax: (803) 725-4233

Abstract

Complex terrain creates small-scale circulations which affect pollen dispersion but may be missed by meteorological observing networks and coarse-grid meteorological models. On volcanic islands, these circulations result from differing rates of surface heating between land and sea as well as rugged terrain. We simulated the transport of bentgrass, ryegrass, and maize pollen from 30 sources within the agricultural regions of the Hawaiian island Kaua'i during climatological conditions spanning season conditions and the La Niña, El Niño, and neutral phases of the El Niño-Southern Oscillation. Both pollen size and source location had major effects on predicted dispersion over and near the island. Three patterns of pollen dispersion were identified in response to prevailing wind conditions: southwest winds transported pollen inland, funneling pollen grains through valleys; east winds transported pollen over the ocean, with dispersive tails for the smallest pollen grains following the mean wind and extending as far as the island of Ni'ihau 35 km away; and northeast winds moved pollen inland counter to the prevailing flow due to a sea breeze circulation that formed over the source region. These results are the first to predict the interactions between complex island terrain and local climatology on grass pollen dispersion. They demonstrate how numerical modeling can provide guidance for field trials by illustrating the common flow regimes present in complex terrain, allowing field trials to focus on areas where successful sampling is more likely to occur.

Keywords: Atmospheric Dispersion; Atmospheric Modeling; Sea Breeze; Zea mays, Argostis sp, Lolium sp.

Introduction

The need for accurate modeling of pollen transport from agricultural regions is underscored by the potential for transgenic pollen to cross-pollinate with compatible conventional or wild varieties. In anemophilous plants such as maize (*Zea mays* L.), the extent of pollen dispersal from male flowers is determined primarily by the direction and speed of the wind. In many cases, particularly in flat terrain, the direction and distance of transport can be predicted from knowledge of the large-scale flow and estimation of the influence of unresolved turbulent motions (Klein et al. 2003; Aylor et al. 2006; Arritt et al. 2007). In contrast to flat terrain, accurate predictions of pollen transport are more challenging in island environments and mountainous regions where differing rates of surface heating and variation in surface drag can create small-scale circulations that deviate from the prevailing winds. Modeling studies by Helbig et al. (2004) found that atmospheric circulations arising from complex topography can act to increase the distance of pollen transport and create undesirable conditions favoring cross-pollination.

The island of Kaua'i in the Hawaiian archipelago is one such environment that contains agricultural regions managed within complex topography surrounded by ocean. The topography of Kaua'i consists of a broad volcanic mountain reaching 1600 m above mean sea level with numerous valleys created by lava flows spreading in all directions from the peak (Macdonald et al. 1983; Fig. 1a). The small-scale meteorological features created by such complex terrain require a concentrated sensor network to resolve adequately. For example, mountains block air flow, resulting either in orographic lift (Lu and Turco 1994) or lateral diversion of the mean wind (Soler et al. 2011). Land-sea breezes which form within a few kilometers of the coast also are common and can reinforce the mean flow or oppose it depending on time of day and location (Liu and Moncrieff 1996). Prevailing winds over Kaua'i are most often from the northeast to southeast (Miller 1981), so sea breezes that run counter to the mean flow on a diurnal cycle are most often observed in the lee of the mountains. Agricultural regions on Kauai can be found along most of the coast with the exception of the northwest coast (Fig. 1b; Melrose 2015). The regions along the southern and western coasts of Kauai are the most extensive and have the greatest inland extent, and are home to the widest range of crops on the island as well as the greatest extent of seed production, which accounts for 63% of Kauai's cropland. One of the fastest-growing agricultural specializations in the Hawaiian Islands (including Kauai) is the seed industry, which has seen well over a tenfold increase in value over the past three decades. Expansion of the seed industry has been encouraged by the islands' year-round growing season which allows multiple crop cycles per year (Loudat and Kasturi 2013).

Although it is not practical to measure all the complex circulations that would affect pollen flow across Kaua'i, tools such as numerical modeling can be used to assess likely patterns and mechanisms of pollen transport. We have studied the potential for complex circulations around the Hawaiian island of Kaua'i to affect pollen dispersion using a fine-scale meteorological model to capture small-scale circulation features and a Lagrangian particle dispersion model to predict pollen movement within the simulated environment. Pollen dispersion was simulated for selected days spanning four consecutive years and three particle sizes to assess the primary wind

patterns and resulting dispersion patterns that could be expected across species and seasonally varying conditions in this island environment. This modeling approach can provide guidance for the design of field studies of pollen dispersal or crop isolation in complex island environments where wind patterns are not easily observed or managed.

Methods

Forecasting local wind patterns

The Weather Research and Forecasting (WRF) Version 3.1 model available from the National Center for Atmospheric Research (*www.wrf-model.org*) was used to predict local meteorological conditions affecting particle dispersion. The WRF model uses time dependent, compressible, non-hydrostatic Euler equations to predict three-dimensional wind and turbulence kinetic energy in terrain-following coordinates.

WRF was configured using three nested domains with grid spacing and time step scaled in a 1:3 ratio between domains. Grid spacing was 4.5 km on the outer domain in order to capture mesoscale circulations and 0.5 km grid on the inner domain in order to represent small-scale, complex circulations with a transition grid of 1.5 km between the two to reduce numerical artifacts resulting from large changes in grid spacing. The model used 27 vertical levels with higher resolution through the lower part of the boundary layer (between 20 and 200 m) to capture near-surface features which have the greatest impact on pollen dispersion. The innermost grid had 447x468 points creating a domain which was 223.5 km in the east-west direction and 234 km in the north-south direction. Dispersion simulations were performed on the innermost grid only since few viable pollen grains would be expected to leave that domain. Simulations began at 2000 local standard time (LST) the evening prior to the day of interest and ran for 24 h. This provided sufficient time to establish atmospheric conditions prior to and during the period of pollen release, which generally occurs from early morning until late afternoon for the pollen types used in this study (Fonseca et al. 2003; Van de Water et al. 2007). Topography was defined using a digital elevation model at 3-second (~90 m) resolution from the Shuttle Radar Topography Mission conducted by the Consultative Group for International Agricultural Research's Consortium for Spatial Information (http://srtm.csi.cgiar.org/index.asp). Land-use information was taken from the 30 s resolution database that accompanies WRF.

The Mellor-Yamada-Janjic (MYJ) planetary boundary layer scheme (Janjic 1990) was used for the two outer domains. The MYJ assumes mechanical production of turbulence kinetic energy is dominated by the vertical shear of the horizontal wind. This assumption is likely to be violated in our innermost domain, where turbulent eddies are partially resolved leading to vertical velocities of comparable magnitude to the horizontal components. Although the fine spacing of the inner domain rendered the simulations computationally demanding, it allowed us to explicitly predict the largest convective structures and to resolve the structure of the sea breeze circulations that form along the coastal regions. Cumulus parameterization was not used because the grid spacing used in our

implementation is too small to satisfy the scale separation assumptions inherent to cumulus parameterization (Weisman et al. 1997)

Initial and lateral boundary conditions were provided by the ERA-Interim Reanalysis dataset available from the European Center for Medium-Range Weather Forecasts (Dee et al. 2011; *www.ecmwf.int*). These data are available at 6-h intervals and a horizontal resolution of 1.5°, which was linearly interpolated to the WRF model grid. Three-dimensional wind and turbulence kinetic energy outputs from WRF were saved at 5-min intervals for input to the dispersion model.

The year-round growing conditions in Hawaii mean that there is no specific pollination date as in mid-latitude locations; thus, our study days need to include a range of meteorological conditions found throughout the year. Meteorological conditions were simulated that represented the main climatological wind patterns present over the island. A climatological analysis of winds for 1981-2010 over Kauai found that East, Northeast, and West were the three primary wind directions present at the Lihue airport (Fig. 2a). Since it is impractical to run multi-year simulations using the fine grid resolution of our model, we chose to examine a sample of days which represented the primary wind patterns. Guided by previous research that shows the climate of Hawaii is affect by both the seasonal cycle and the El Niño-Southern Oscillation (ENSO) cycle (e.g., Lyons 1982) we selected 14 evenly-spaced days between January 2005 and April 2008 that spanned both the seasonal cycle and the neutral, El Niño, and La Niña phases of ENSO (NOAA 2012). The days selected were 15 Jan, 15 Apr, 15 Jul, and 15 Oct of 2005-2007, and 15 Jan and 15 Apr 2008. Analysis of the wind conditions on these days show that 12 of the 14 days in our analysis consisted of northeast or easterly winds, matching the climatology of the region (Fig. 2b; Table 1). The remaining two days exhibited predominantly south or southwest winds.

Predicting Particle Dispersion

Three-dimensional movement of hypothetical tracer particles was simulated with a Lagrangian Particle Dispersion Model developed by Arritt et al. (2007). The mean and turbulent wind components used by the model are given by

$$x_{ik}(t+dt) = x_{ik}(t) + [u_{ik}(t) + u_{0ik}(t)] \qquad k = 1, 2, 3 \tag{1}$$

where x_{ik} is the position of the i^{th} particle in the k dimension, u_{ik} is the mean wind that the particle experiences, and u_{0ik} is a simulated random component of the wind to account for unresolved turbulence. The model time step was dt = 2 s. The value of u_{0ik} was calculated as a first-order Markov process

$$u_{0ik}(t+dt) = u_{0ik}(t)R_{ik}(dt) + [1 - R_{ik}(dt)^2]^{1/2} q\sigma_{ik} \qquad k = 1, 2, 3 \tag{2}$$

where R_{ik} is the autocorrelation value, q is a normally distributed random number with the distribution N(0,1), and σ_{ik} is the standard deviation of the wind speed in the k dimension (McNider et al. 1988) which is estimated from the modeled turbulence kinetic energy field (Garratt 1992; MacInnes and Braco 1992). R_{ik} acts as a memory of turbulent motion at the previous time step and is determined by the particle's Lagrangian timescale in the k dimension, Γ_{ik}

$$R_{ik}(dt) = \exp\left(\frac{-dt}{\Gamma_{ik}}\right) \tag{3}$$

As R_{ik} decreases from 1 to 0 a particle's turbulent motion goes from constant in time to completely random.

In the horizontal dimensions we assume that the particle timescale equals the fluid timescale, and is given by

$$\Gamma_{ik} = \frac{x_{i3}(t)}{2\sigma_{ik}} \qquad \text{k = 1,2} \tag{4}$$

In the vertical dimension, pollen grains require additional terms in the equations for turbulent motions in order to account for their terminal velocity. In the vertical dimension the particle timescale will not be equal to the fluid timescale because heavy particles lose memory faster than the flow (Csanady 1963). Instead, the particle timescale in the vertical dimension is given as

$$\Gamma_{i3} = \frac{x_{i3}(t)}{2\sigma_{i3}\sqrt{1+\left(\beta v_T/\sigma_{i3}\right)^2}} \tag{5}$$

where v_T is the particle's terminal fall speed in still air and β is a dimensionless coefficient set to 1.5.

The drift correction term (w_c) was added to the vertical component of the particle's motion (Legg and Raupach 1982) and is defined as

$$w_c = \frac{x_{i3}(t)}{2\sigma_{i3}}\frac{\partial(\sigma_{i3}^2)}{\partial z}\left[1 - R_{i3}(\Delta t)\right] \tag{6}$$

Failure to include the drift term results in particles accumulating in regions of low turbulent intensity, which is counter to observations (Legg and Raupach 1982; MacInnes and Bracco 1992). Thus, the drift correction term preserves the well-mixed condition. Terminal fall speed is also added to the vertical velocity and is prescribed based on the particle size following Stokes' Law, so that Eq. 1 becomes

$$x_{ik}(t+dt) = x_{ik}(t) + \left[u_{ik}(t) + u_{0ik}(t) + \delta_{k3}(w_c - v_T)\right]dt \tag{7}$$

We chose three well established grass species [bentgrass (*Agrostis* sp.), ryegrass (*Lolium* sp.), and maize (*Zea mays* L.)] as representative pollen types spanning a range of pollen sizes for this study. All three species were introduced for agricultural purposes (Ripperton et al. 1933; Daehler 2005; USDA-NASS) and have been subject of numerous studies on pollen dispersion (Arritt et al. 2007; Astini et al. 2009; Giddings 2000; Van de Water et al. 2007). Their pollen sizes and settling velocities span the range of most grass species: bentgrass (*Agrostis* sp.) pollen [~25 µm; v_t = 0.02 ms^{-1}; Pfender et al. (2007); Van de Water et al. (2007)], ryegrass (*Lolium* sp.) pollen

[~50 µm; v_t = 0.09 ms^{-1}; Jansen and Den Nijs (1993); Humphreys et al. (2010)] and maize (*Zea mays* L.) pollen[~100 µm; v_t = 0.37 ms^{-1}; Stanley and Linskens (1974); Johnson and Mulcahy (1978); Aylor, (2002)]. The location of thirty pollen sources was specified in a grid with spacing at 2.5 km intervals along the southern and western edges of the island where intensive seed production operations are located. Simulated bentgrass and ryegrass pollen grains were released at a height of 1.05 m, which approximates the height of taller panicles of these grasses (Miller 1984); maize pollen was released at 2 m, a common height for commercial maize tassels (Abendroth et al 2011).

For maize, the same number of particles were emitted at each source but were distributed in a diurnally varying pattern using the pollen shed model of Viner et al. (2010) which describes the rate of pollen shed at any time during the day as a function of the incoming solar radiation, vapor pressure deficit of the atmosphere, and the air temperature which are taken from the meteorological simulations. The model simulates the process of anther drying during the course of the day which leads to an increase in pollen shed through the morning as additional anthers dry and open followed by a decrease in pollen shed through the afternoon as the anthers become depleted of their pollen. The actual amount of pollen could be calculated by scaling the model results using typical rates of pollen shed from each crop (Fonseca et al., 2003; Astini et al. 2009). Assuming a typical plant density for maize of 12.5 plants m^{-2}, simulated pollen released would represent about 10^{-6} to 10^{-7} of the actual amount of pollen that might be produced in a maize field, based on pollen production estimates from Uribelarrea et al. (2002). Bentgrass also exhibits a diurnally varying rate of pollen shed (Pfender et al. 2007) although the environmental factors which influence the rate of pollen shed are not known for bentgrass. To capture a diurnally varying pattern, we created a diurnal pattern based on the relative rates of pollen shed illustrated in Figure 3 of Pfender et al. (2007) with pollen shed beginning at sunrise and ending at sunset. The same pattern of bentgrass pollen shed was used for each model day. For ryegrass, there was insufficient published literature to develop diurnal shed models for these species. Therefore, a constant rate of pollen shed was released from each source at each timestep between sunrise and sunset, resulting in ~560,000 particles in each simulation (~14,500 per source). We assumed that no pollen shed occurred from ryegrass during the night. Because bentgrass and ryegrass have much higher plant densities, the modeled pollen release may represent an even smaller fraction of actual pollen production compared to maize.

A primary mechanism for lofting pollen out of the canopy is convective updrafts, commonly referred to as ejection events. The model grid directly predicts large-scale convective structures, but does not predict the fine-scale turbulent motions that might exist within and above the plant canopies from which pollen is shed. For these turbulent motions, we relied on the parameterized turbulence from the meteorological model which is used to calculate the random motion component portion of pollen transport in the pollen transport model.

Particles were considered deposited when they passed through a plane approximating the lower limit of receptive flower height for each species. This was 1.0 m above the surface for maize and ryegrass, and 0.5 m for bentgrass (Abendroth et al. 2011; Daehler 2005; Humphreys 2010). The deposition calculation ignores possible rebound or re-suspension of particles after deposition (Aylor 1985). Previous simulations without this correction,

however, have provided estimates of maize pollen dispersal in agreement with field observations (Astini et al. 2009). All predictions of pollen dispersion also included an estimate of viability at the time of deposition (Viner and Arritt 2010). For maize, we applied the viability model developed by Fonseca and Westgate (2005); bentgrass and ryegrass viabilities were restricted to a three-hour period following Fei and Nelson (2003) and Wang et al. (2004). Based on prevailing atmospheric conditions and duration of pollen transport on the days of simulation, bentgrass, ryegrass, and maize pollen would not have lost significant viability between shed and deposition (data not shown).

Results

Simulation of Wind speed and Direction

Measurements of surface wind speed and direction taken from an Automated Surface Observing Station (ASOS) at Lihue Airport (LIH; 21.98°N, 159.35°W) were used to evaluate the WRF simulations of surface meteorological conditions over Kaua'i. A summary of the measured wind conditions at Lihue airport on the 14 days is shown in Figure 2, with a summary of the average wind speed and direction listed in Table 1. Twelve of the days exhibited winds that were directed from the northeast or east, which is typical for Northern Hemisphere tropical trade wind regimes. Two simulated days, 15 Jan 2005 and 15 Oct 2006, reflected different wind patterns with winds from the south or southwest during the day.

Comparing the hourly averaged simulated wind conditions to the corresponding measurements shows that the WRF simulations provided a fairly accurate depiction of wind speeds and directions at the Lihue airport (Fig. 3). Measured surface winds by the ASOS were most frequent between north and east (0 to 90°) and greater than 4 m s^{-1}. Simulated winds, however, tended to be several degrees to the north of measured wind directions in this range, and 1 to 2 m s^{-1} faster than measured winds for measured values above 4 m s^{-1}.

Statistical analysis of simulated and measured wind speed and direction for the 14 selected days generated Root Mean Square Error values of $RMSE_{spd}$ = 1.35 m s^{-1} and $RMSE_{dir}$ = 33.4° . Errors in simulated wind direction reflect the model's under-prediction of southerly and (to a lesser extent) westerly winds. We believe this was due to influence of the Ha'upu Ridge to the south and west of Lihue airport, which was not adequately resolved by the WRF model despite the high-resolution topography used in our simulation. Afternoon wind profiles also were compared to the 00 UTC LIH soundings. Again, WRF tended to over-predict wind speeds by 1 to 2 m s^{-1}, and produced more southerly wind directions at elevations above 0.5 km ($RMSE_{spd}$ = 1.08 ms^{-1}; $RMSE_{dir}$ = 23.7°).

Simulation of Pollen Dispersion

Three distinct patterns of pollen dispersion were identified based on the three prevailing wind patterns (from the northeast, east, and south/southwest). Three of the 14 simulated days will be used to depict the three

patterns of dispersion. Results for 15 Apr 2006 illustrate dispersion under prevailing east winds, 15 Jul 2005 illustrates dispersion under northeast winds, and 15 Jan 2005 illustrates dispersion during prevailing south/southwest winds.

In the case with east winds (Case 'E'), pollen was predominantly transported off the island and over the ocean (Fig. 4). On these days, pollen grains traveling less than 1 km from their source were deposited over land. Those traveling between 1 and 35 km were generally deposited over the coast and ocean, and those traveling greater than 35 km had the potential to reach the neighboring island of Ni'ihau. Pollen types of all three sizes were transported tens of kilometers. Very few of the larger pollen grains travelled such distances, while more of the smaller pollen grains remained aloft long enough to reach Ni'ihau.

In the case with southwest winds (Case 'SW'), pollen was transported towards the island's interior (Fig. 5). On these days, pollen grains falling within 35 km of the source were generally deposited on land while those travelling over 35 km were dispersed over the ocean beyond the far side of the island. Pollen transport under these wind conditions was noticeably more limited, particularly for larger pollen grains with very few of the 50 or 100 μm pollen grains being transported more than a few hundred meters. The 25 μm pollen grains were transported a greater distance, comparable to the 'E' case, but much of the pollen that traversed over land was deposited in the interior valleys of Kaua'i. Pollen from sources near the eastern and western edges of the source region was transported by winds passing around the exterior of the mountains and travelled beyond the island.

The northeast winds case on 15 Jul 2005 (Case 'NE') was similar to the 'E' case, but shifting of the wind was sufficient to allow a sea breeze to develop over the source region (Fig. 6). Pollen grains released along the southwest and western coasts in this situation were transported inland counter to the prevailing northeast wind (Fig. 7). In these cases, deposition typically was limited to within 10 km of the source. Some of the pollen was lifted by updrafts created by convergence of the sea breeze and the mean flow, and consequently recirculated back to the west coast. Recirculation was particularly prevalent for smaller particles, which did not settle as quickly and were readily lifted by updrafts. In these situations, recirculation due to the sea breeze limited the distance pollen dispersed from the sources.

Discussion

We have applied a combination of meteorological and Lagrangian dispersion modeling to examine potential dispersal patterns for various particle sizes on the Hawaiian island of Kaua'i. This location is a challenge for predicting pollen dispersion because its complex topography and surrounding ocean create small-scale circulations that may not be detected by conventional meteorological sensing networks. Our numerical modeling approach provided a physically-based assessment of the local meteorological conditions that control pollen dispersion. By examining the typical range of climate variations encountered on the island and a range of pollen grain sizes common in agriculture, we have generated a basic characterization of pollen dispersion expected from wind-pollinated crops in this environment.

Three distinct patterns of pollen dispersion were identified during the simulated dates, primarily caused by the complex terrain and the location of sea breezes around the island of Kaua'i. Prevailing winds were most often from the northeast or the east. Small shifts in the prevailing winds to the northeast produced very different patterns of dispersion resulting from a sea breeze flow occurring over the source region that directed pollen flow inland. In contrast, a small shift to the east moved the sea breeze flow away from the source region. This allowed pollen to be captured by the prevailing winds and transported over the ocean and to the island of Ni'ihau.

For southwesterly prevailing winds, the complex terrain generated a number of situations resulting in preferential pollen deposition or dispersal. Rapidly rising topography acted as a physical barrier to pollen flow for transport through the interior of the island. Even gradually rising topography across the source region acted as a barrier to transport of larger pollen grains due to their greater terminal fall speeds. For smaller pollen grains, vertical motion generated by the WRF model appears to have been sufficient to prevent rising topography within the source region from impeding transport. Pollen directed toward the island's interior, however, was preferentially channeled through valleys where it was deposited within and along the sides of the valleys. For easterly prevailing winds, similar deposition behavior was seen in the model for 25 μm particles reaching the neighboring island Ni'ihau; most of these particles were deposited at the base of a ridge on the windward side of that island (Fig. 8).

The preferential deposition of pollen on windward slopes simulated here contrasts with previous results for bentgrass pollen deposition in the complex terrain of central Oregon (Viner and Arritt 2012). In that study, predicted deposition of 25 μm bentgrass pollen was greater on the lee slopes. Results from Lehning et al. (2008) provide a possible explanation for differences in the amount of deposition occurring on windward and leeward slopes of complex terrain for particles ranging from 10 to 100 μm. Their results suggest that the amount of deposition is decreased on windward slopes of mountains due to convergence of the wind, which produces rising motions and increased on leeward slopes due to divergence of the wind, which produces downward motions. Conversely, wind tunnel and computational fluid dynamics simulations described by Parker and Kinnersley (2004) showed deposition maxima on the windward side of an obstacle. In addition, Goosens (2006) showed that particle deposition over an obstacle was affected by details of the local topography, such as whether a slope is concave or convex. Clearly, more work is necessary to understand the impact of terrain slopes on pollen dispersion and deposition.

Specific combinations of terrain and wind direction can have strong effects on pollen dispersion. Closer examination of pollen transport in the case of easterly prevailing winds showed that most long-range transport of 50 and 100 μm pollen grains originated from three sources located on higher elevations with a steep downward slope in the direction of the mean wind; very few pollen grains from the other 27 sources were transported more than a few kilometers (Fig. 9). Evidently, this combination of elevation and slope allowed more pollen grains to remain airborne and be lifted by updrafts before reaching the deposition height. Pollen grains released from sources located nearby on flatter terrain were deposited within several meters of their sources under the same

conditions. This result is consistent with our findings for the case with southwesterly prevailing winds, where most of the larger pollen grains were quickly deposited as they were transported inland and upslope. In that case some pollen was deposited in the lee of the mountains, generally originating from sources near the western and eastern edges of the source region. We hypothesize this outcome resulted from the sea breeze on the northeast side of the island in the lee of the mountains flowing counter to the prevailing wind. Simulated pollen grains transported around the east side of the mountains were caught by the sea-breeze flow and pushed back into the island, where they were deposited on the lee of the mountains relative to the synoptic flow. This behavior was not found when pollen was transported around the western side of the island, where it remained within the prevailing flow and was not affected by the sea breeze.

Pooling dispersion data across all simulations, the smallest pollen grains (25 μm) travelled much farther than larger grains, consistent with their slower terminal fall speed (Fig. 10). Heavier particles (50 and 100 μm) had much steeper deposition profiles with distance from the sources, with 50 and 100 μm particles showing similar patterns. Averaged across 14 days of simulation, 87.7% of 25 μm particles, 98.9% of 50 μm particles, and 99.8% of 100 μm particles were deposited within 10 m of their sources. About 10% of the 25 μm particles travelled more than 1 km and about 2% could have reached the neighboring island of Ni'ihau about 35 km to the west; 50 and 100 μm grains rarely if ever travelled that distance. For the case with easterly prevailing winds, 2 to 3% of 25 μm pollen grains were transported to Ni'ihau, while less than 0.2% of 100 μm particles travelled more than 10 m beyond their source. This disparity in transport was particularly evident when pollen was directed inland, either due to prevailing flow from the southwest or the sea breeze recirculation with wind from the northeast. In the easterly wind case release of pollen from only a few sources resulted in deposition greater than a few hundred meters downwind. These results underscore the dominant influence of topography in determining the dispersion pattern for large pollen grains. Even 25 μm pollen dispersion was largely confined to valleys and windward slopes under these conditions.

Creating an ensemble of likely pollen dispersion outcomes for a variety of climatologically-representative conditions and pollen shed intensities could be useful in minimizing outcrossing in open-pollinated crops grown on the island. While the results shown here do not account for all scenarios, it can be extended for specific crops during periods associated with known peaks in pollen production or especially sensitive conditions. Model predictions would not have to be repeated unless climatological wind statistics over the location change sufficiently to warrant re-evaluation. Finally, the approach used here could be used to inform the design of field experiments to measure pollen dispersion in complex terrain or along coastlines. Our results indicate there are complex interactions between pollen aerodynamics (as represented by terminal velocity) and small-scale atmospheric circulations but little data are available to validate the results. This is hampered by the difficulty and expense of performing field studies in these regions. With the assistance of numerical modeling the areas of interest can be focused down to a few regions, making field studies more efficient and more likely to be successful.

Acknowledgements

This project was supported by Biotechnology Risk Assessment Program Grant numbers 20073921118473 and 20093352205804 from the United States Department of Agriculture's National Institute of Food and Agriculture (NIFA). Computing resources were funded by an endowment to the Department of Agronomy at Iowa State University. We thank Daryl Herzmann for computing assistance.

References

Abendroth LJ, Elmore RW, Boyer MJ, Marlay SK (2011). Corn Growth and Development. PMR 1009. Iowa State University Extension, Ames, IA.

Arritt RW, Clark CA, Goggi AS, Sanchez HL, Westgate ME, Riese JM (2007) Lagrangian numerical simulations of canopy air flow effects on maize pollen dispersal. Field Crops Res. 2:151-162.

Astini JP, Fonseca A, Clark CA, Lizaso J, Grass L, Westgate ME, Arritt RW (2009) Predicting out-crossing in maize hybrid seed production. Agronomy J. 101: 373-380.

Aylor DE, Ferrandino FJ (1985) Rebound of pollen and spores during deposition on cylinders by inertial impaction. Atmos. Environ. 19:803-806.

Aylor DE (2002) Settling speed of corn (Zea mays) pollen. J. Aerosol Sci. 33:1601-1607.

Aylor DE, Boehm MT, Shields JE (2006) Quantifying aerial concentrations of maize pollen in the atmospheric surface layer using remote-piloted airplanes and Langrangian stochastic modeling. J. Appl. Met. And Climatology. 45:1003-1015.

Csanady GT (1963) Turbulent diffusion of heavy particles in the atmosphere. J. Atmos. Sci. 20:201-208.

Daehler CC (2005) Upper montane plant invasions in the Hawaiian islands. Perspectives Plant Ecology, Evolution, Systematics 7: 203-216.

Dee DP, Uppala SM, Simmons AJ et al (2011) The ERA-Interim reanalysis: configuration and performance of the data assimilation system. Quarterly J. Royal Met. Soc. 137:553-597.

Fei S, Nelson E (2003) Estimation of pollen viability, shedding pattern, and longevity of creeping bentgrass on artificial media. Crop Sci. 43:2177-2181.

Fonseca AE, Westgate ME, Grass L, Dornbos DL Jr (2003) Tassel morphology as an indicator of potential pollen production in maize. Crop Manag. doi:10.1094/CM-2003-0804-01-RS.

Fonseca AE, Westgate ME (2005) Relationship between desiccation and viability of maize pollen. Field Crops Res. 94:114-125.

Garratt JR (1992) The atmospheric boundary layer. Cambridge University Press. 316 pp.

Giddings G (2000) Modelling the spread of pollen from *Lolium perenne*. The implications for the release of wind-pollinated transgenics. Theor. Appl. Genet 100:971-974.

Goosens D (2006) Aeolian deposition of dust over hills: the effect of dust grain size on the eposition pattern. Earth Surf Process Landforms. 31:762-776.

Helbig N, Vogel B, Vogel H, Fiedler F (2004) Numerical modelling of pollen dispersion on the regional scale. Aerobiologia 20:3-19.

Humphreys M, Feuerstein U, Vandewalle M, Baert J (2010). Ryegrass. Ch 10. In: B Boller, UK Posselt, F Veronesi (eds). Fodder Crops and Amenity Grasses. Springer.

1 Janjic ZI (1990) The step-mountain coordinate: Physical package. Mon. Weather Rev. 118:1429-1443.

2 Jansen RC, Den Nijs APM (1993) A statistical mixture model for estimating the proportion of unreduced pollen
3 grains in perennial ryegrass (*Lolium perenne* L.) via the size of pollen grains. Euphytica 70:205-215.

4 Johnson CM, Mulcahy DL (1978) Male gametophyte in maize II: Pollen vigor in inbred plants. Theor. Appl. Genet.
5 51:211-215.

6 Klein EK, Lavigne C, Foueillassar X, Gouyon PH, Laredo C (2003) Corn pollen dispersal: quasi-mechanistic models
7 and field experiments. Ecol. Mon. 73:131-150.

8 Legg BJ, Raupach MR (1982) Markov-chain simulation of particle dispersion in inhomogeneous flows: the mean
9 drift velocity induced by a gradient in Eulerian velocity variance. Boundary Layer Met. 24:3-13.

10 Lehning M, Lowe H, Ryser M, Raderschall N (2008) Inhomogeneous precipitation distribution and snow transport in
11 steep terrain. Water Resources Res. 44:W07404.

12 Liu CH, Moncrieff MW (1996) A numerical study of the effects of ambient flow and shear on density currents.
13 Mon. Weather Rev. 124:2282-2303.

14 Loudat T, Kasturi P (2013) Hawaii's seed crop industry: Current and potential economic and fiscal contributions.
15 Report prepared for Hawaii Farm Bureau Federation, 8 pp.

16 Lu R, Turco RP (1994) Air pollutant transport in a coastal environment Part 1: 2-dimensional simulations of sea-
17 breeze and mountain effects. J Atmos Sci. 51-2285-2308.

18 Lyons SW (1982) Empirical orthogonal function analysis of Hawaiian rainfall. J. Appl. Meteor. 21:1713-1729.

19 Macdonald GA, Abbott AT, Peterson FL (1983) Volcanoes in the sea: the geology of Hawaii. University of Hawaii
20 Press, Hawaii.

21 MacInnes JM, Bracco FV (1992) Stochastic particle dispersion modeling and the tracer-particle limit. Phys. Fluids.
22 A4:2809-2824.

23 McNider RT, Moran MD, Pielke RA (1988) Influence of diurnal and inertial boundary layer oscillations on long-
24 range dispersion. Atmos. Environ. 22:2448-2462.

25 Melrose J, Perroy R, Cares S (2015) Statewide agricultural land use baseline 2015. Hawai'I Department of
26 Agriculture. 101pp.

27 Miller DA (1984). Forage crops. New York (NY): McGraw-Hill Inc. 530 p.

28 Miller JM (1981) A 5-year climatology of back trajectories from the Mauna-Loa Observatory, Hawaii. Atmos.
29 Environ. 15:1553-1558.

30 NOAA. National Oceanic and Atmospheric Administration. Climate Prediction Center – Monitoring and Data: ENSO
31 Impacts on the U. S. – Previous Events.
32 http://www.cpc.ncep.noaa.gov/products/analysis_monitoring/ensostuff/ensoyears.shtml. Accessed April
33 12, 2012.

1 Parker ST, Kinnersley RP (2004) A computational and wind tunnel study of particle dry deposition in complex
2 topography. Atmos. Environ. 38:3867-3878.

3 Pfender W, Graw R, Bradley W, Carney M, Maxwell L (2006) Use of a complex air pollution model to estimate
4 dispersal and deposition of grass stem rust urediniospores at landscape scale. Agric. For. Meteorol.
5 139:138-153.

6 Pfender W, Graw K, Bradley W, Carney M, Maxwell L (2007) Emission rates, survival, and modeled dispersal of
7 viable pollen of creeping bentgrass. Crop Sci. 47:2529-2539.

8 Ripperton JC, Goff RA, Edwards DW, Daves WC (1933) Range grasses in Hawaii. Hawaii Agric. Exp. Sta. Bulletin No.
9 65.

10 Soler MR, Arasa R, Merino M, Olid M, Ortega S (2011) Modelling local sea-breeze flow and associated dispersion
11 patterns over a coastal area in North-East Spain: a case study. Boundary Layer Met. 140:37-56.

12 Stanley RG, Linskens HF (1974) Pollen – Biology, biochemistry, management. Springer-Verlag, 307pp.

13 Uribelarea M, Carcova J, Otegui ME, Westgate ME (2002) Pollen production, pollination dynamics, and kernel set in
14 maize. Crop Sci. 42:1910-1918.

15 USDA-NASS. National Agricultural Statistics Service. www.nass.usda.gov/Statistics_by_State/Hawaii/
16 Publications/Annual_Statistical_Bulletin/

17 Van de Water PK, Watrud LS, Lee EH, Burdick C, King A (2007) Long-distance GM pollen movement of creeping
18 bentgrass using modeled wind trajectory analysis. Ecological Appl. 17:1244-1256.

19 Viner BJ, Arritt RW (2010) Increased pollen viability resulting from transport to the upper boundary layer. Field
20 Crops Res. 119:195-200.

21 Viner BJ, Westgate ME, Arritt RW (2010) A model to predict diurnal pollen shed in maize. Crop Sci. 50:235-245.

22 Viner BJ, Arritt RW (2012) Small-scale circulations caused by complex terrain affect pollen deposition. Crop Sci.
23 52:904-913.

24 Wang ZY, Ge Y, Scott M, Spangenberg G (2004) Viability and longevity of pollen from transgenic and nontransgenic
25 tall fescue (*Festuca Arundinacea*) (Poaceae) plants. Am J Bot. 91:523-530.

26 Weisman ML, Skamarock WC, Klemp JB (1997) The resolution dependence of explicitly modeled convective
27 systems. Mon Weather Rev. 125:527-548.

Figure Captions

Fig 1 (a) The island of Kauai within the Hawai'ian islands. The inset indicates the topographical features of Kauai. (b) The island of Kauai with shaded agricultural regions. Particle sources were placed along the southern and western coasts, in the lowest 200 m of elevation.

Fig 2 Wind roses for Lihue, Hawaii summarizing a) the climatological summary of winds in Lihue between 1981 and 2010 where concentric rings give percentage of observations for each speed and direction, at 7% intervals and b) near-surface wind speed and direction from 06 to 18 local time on each date (approximately sunrise to sunset) where concentric rings give percentage of observations for each speed and direction, at 20% intervals.

Fig 3 Comparison of observed surface wind speed (left) and direction (right) at the ASOS meteorological reporting station in Lihue, HI and the corresponding simulated wind speed and direction at the nearest model grid point from the innermost domain. The solid line represents an exact match between the observed and simulated wind speed or direction.

Fig 4 Magnitude of particle deposition in units of particles per m^{-2} normalized by the total number of released particles. Images depict flow from the East on 15 Apr 2006 for particle sizes of 25 µm (top), 50 µm (middle) and 100 µm (bottom).

Fig 5 Magnitude of particle deposition in units of particles per m^{-2} normalized by the total number of released particles. Images depict flow from the Southwest on 15 Jan 2005 for particle sizes of 25 µm (top), 50 µm (middle) and 100 µm (bottom; all particles deposited in close proximity to their source).

Fig 6 Vertical cross-section of wind streamlines in the along-wind and vertical directions depicting sea breeze on the Western coast of Kauai at 22 UTC on 15 Apr 2006. The low-level sea breeze below 500 m is seen to move counter to the mean flow above 1000 m. The cross section is taken at y = 0 km and the x-axis is labeled in terms of distance from the center of Kaua'i (see Fig. 1). Upward motion is strongest over the coastal agricultural plain between -22 and -19 km.The solid black line represents the topography elevation with the coast located at -22 km.

Fig 7 Magnitude of particle deposition in units of particles per m^{-2} normalized by the total number of released particles. Images depict flow from the Northeast on 15 Jul 2005 for particle sizes of 25 µm (top), 50 µm (middle) and 100 µm (bottom; all particles deposited in close proximity to their source).

Fig 8 High-resolution images of deposition of 25 µm particles on the windward side of complex terrain for the ridge on the northeastern coast of Ni'ihau (top) and valleys on the west side of Kauai (bottom). Shaded areas represent the number of particles deposited per m^{-2} normalized by the total number of particles released (darker areas indicate greater particle deposition). Contours indicate 100m changes in elevation with ticks indicating the downhill direction. Distance is measured from the center of Kaua'i (see Fig. 1).

Fig 9 Deposition from three sources (indicated with dark circles) located on steeper leeward slopes (top) and all other sources (bottom). Deposition is given in units of particles per m^{-2} normalized by the total number of particles released.

Fig 10 Proportion of 25, 50, and 100 µm pollen grains deposited at various distances from the sources. Data are the average for all sources and 14 simulation dates.

Table 1: Summary of average wind speed and direction for each of the 14 simulated days.

Date	Wind speed ($m\ s^{-1}$)	Wind direction (degrees from North)
15 Jan 2005	10.7	221
15 Apr 2005	7.0	45
15 Jul 2005	6.9	16
15 Oct 2005	4.3	87
15 Jan 2006	3.2	47
15 Apr 2006	8.4	67
15 Jul 2006	7.7	35
15 Oct 2006	3.6	245
15 Jan 2007	6.4	71
15 Apr 2007	8.0	66
15 Jul 2007	7.6	42
15 Oct 2007	5.7	58
15 Jan 2008	6.4	59
15 Apr 2008	6.2	103

a)

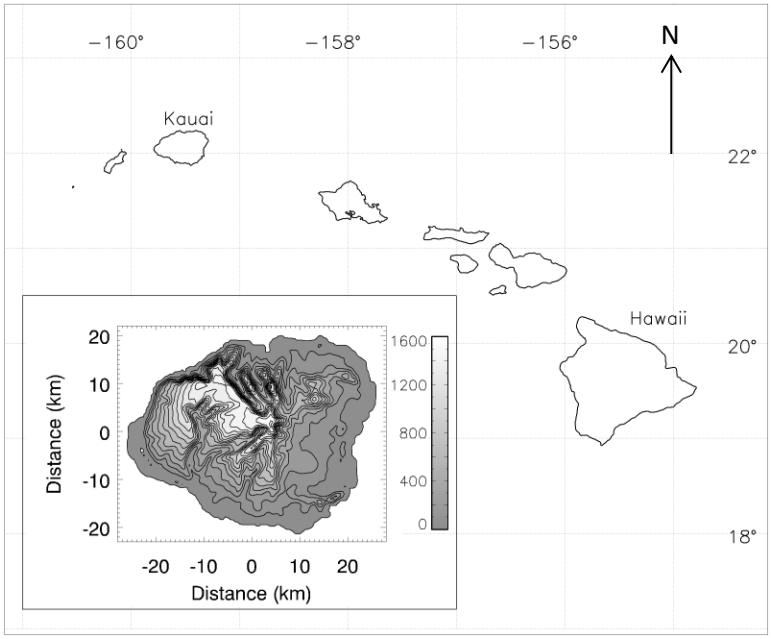

1

b)

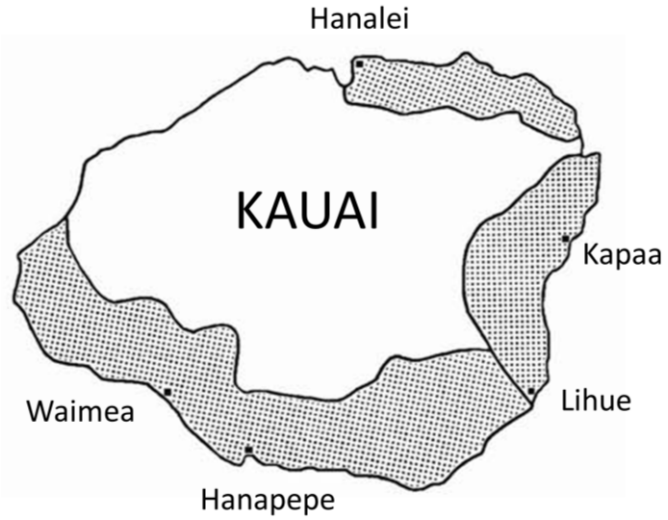

2

3 Figure 1

4

a)

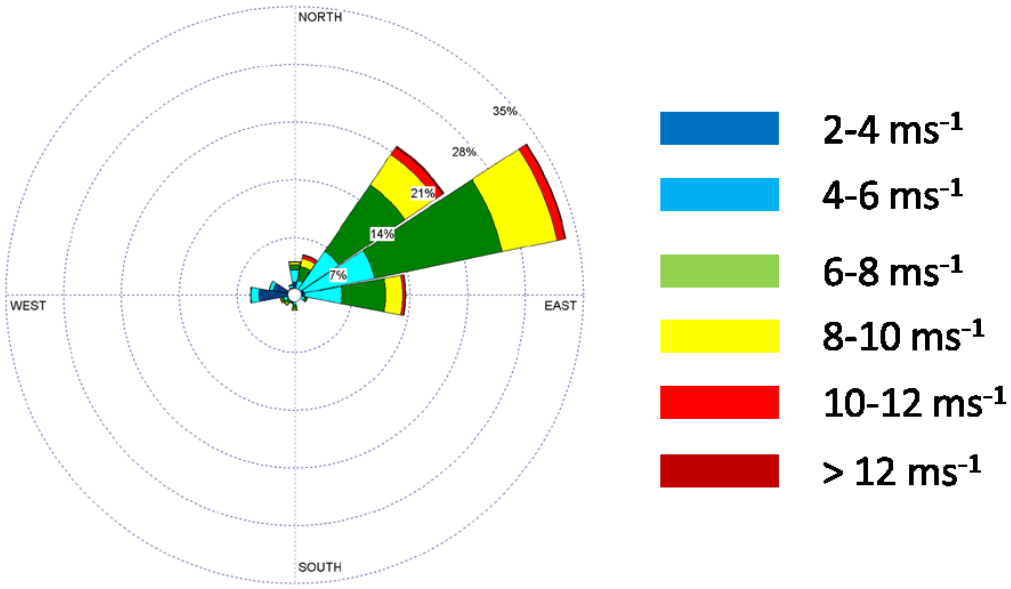
NORTH
WEST
EAST
SOUTH
35%
28%
21%
14%
7%
2-4 ms-1
4-6 ms-1
6-8 ms-1
8-10 ms-1
10-12 ms-1
> 12 ms-1

b)

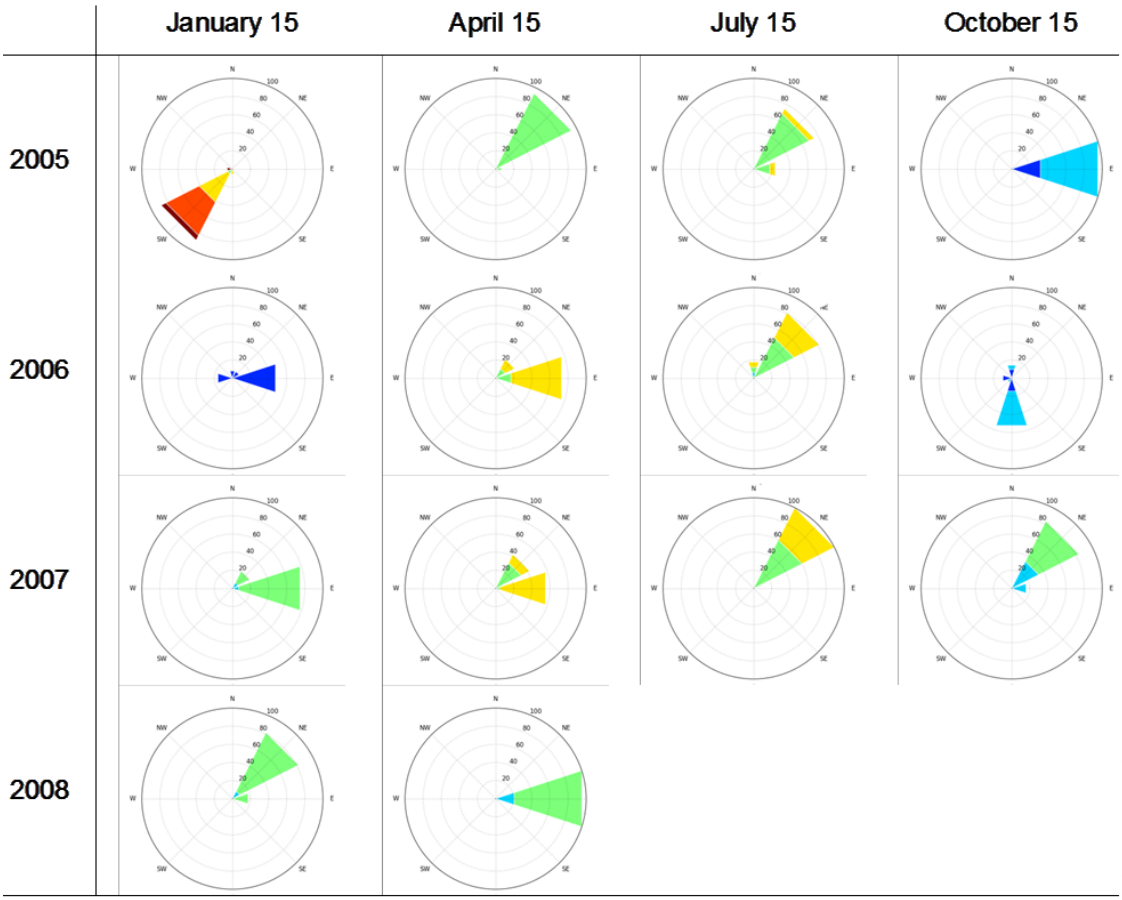
January 15
April 15
July 15
October 15
2005
2006
2007
2008

Figure 2

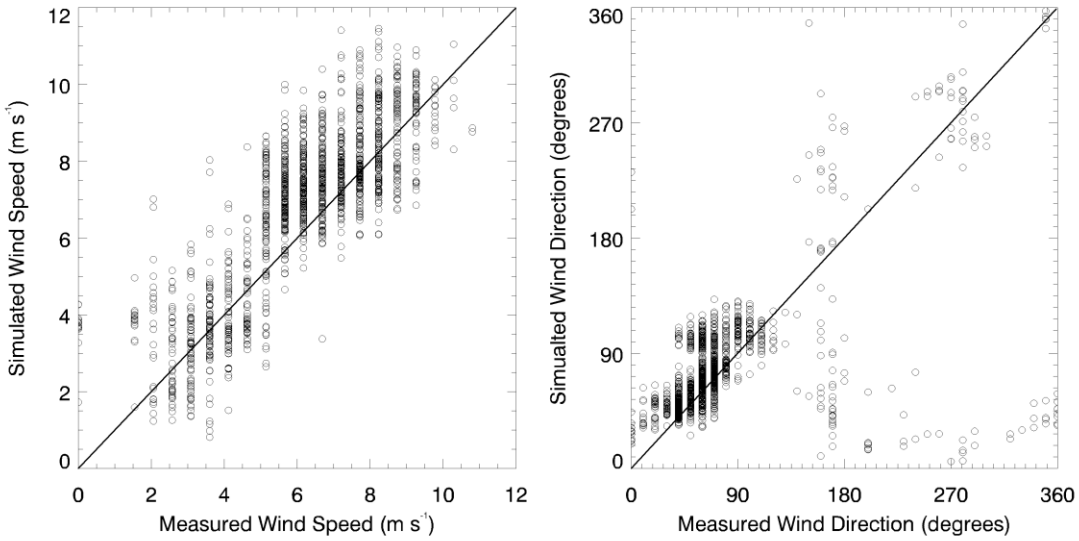
Simulated Wind Speed (m s-1)
Measured Wind Speed (m s-1)
0
2
4
6
8
10
12
Simualted Wind Direction (degrees)
Measured Wind Direction (degrees)
0
90
180
270
360

Figure 3

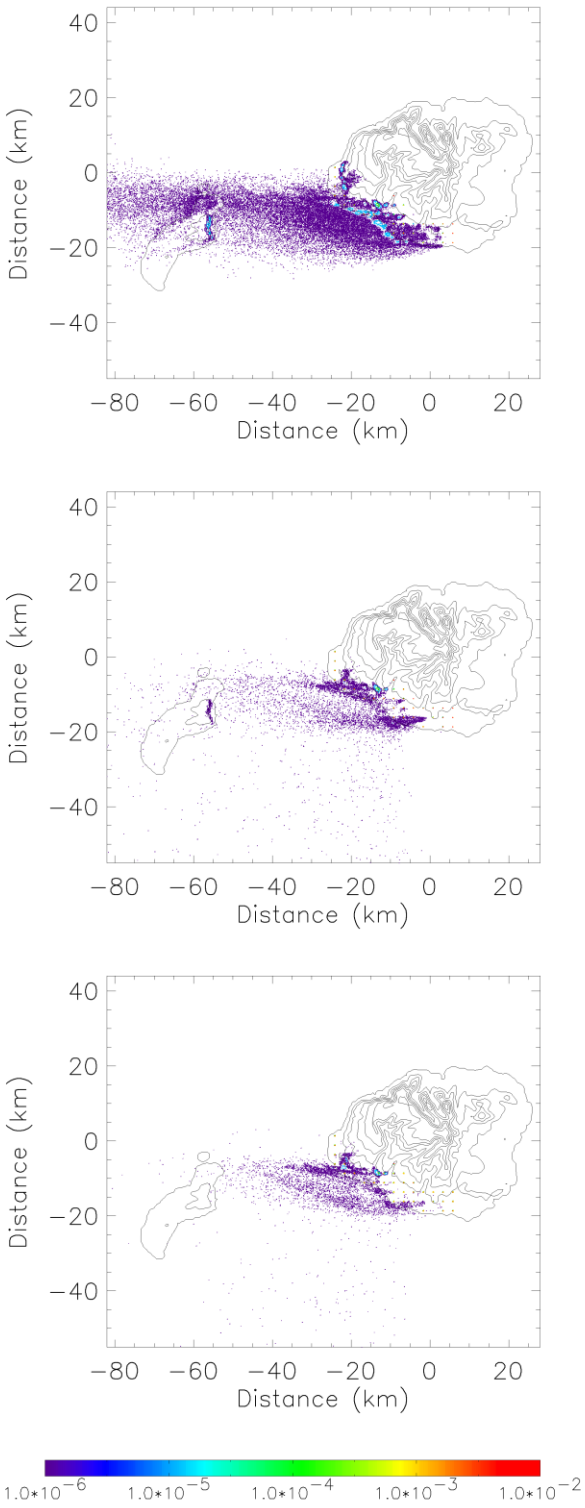
40
20
0
−20
−40
Distance (km)
−80 −60 −40 −20 0 20
Distance (km)
1.0*10^−6
1.0*10^−5
1.0*10^−4
1.0*10^−3
1.0*10^−2

1

2 Figure 4

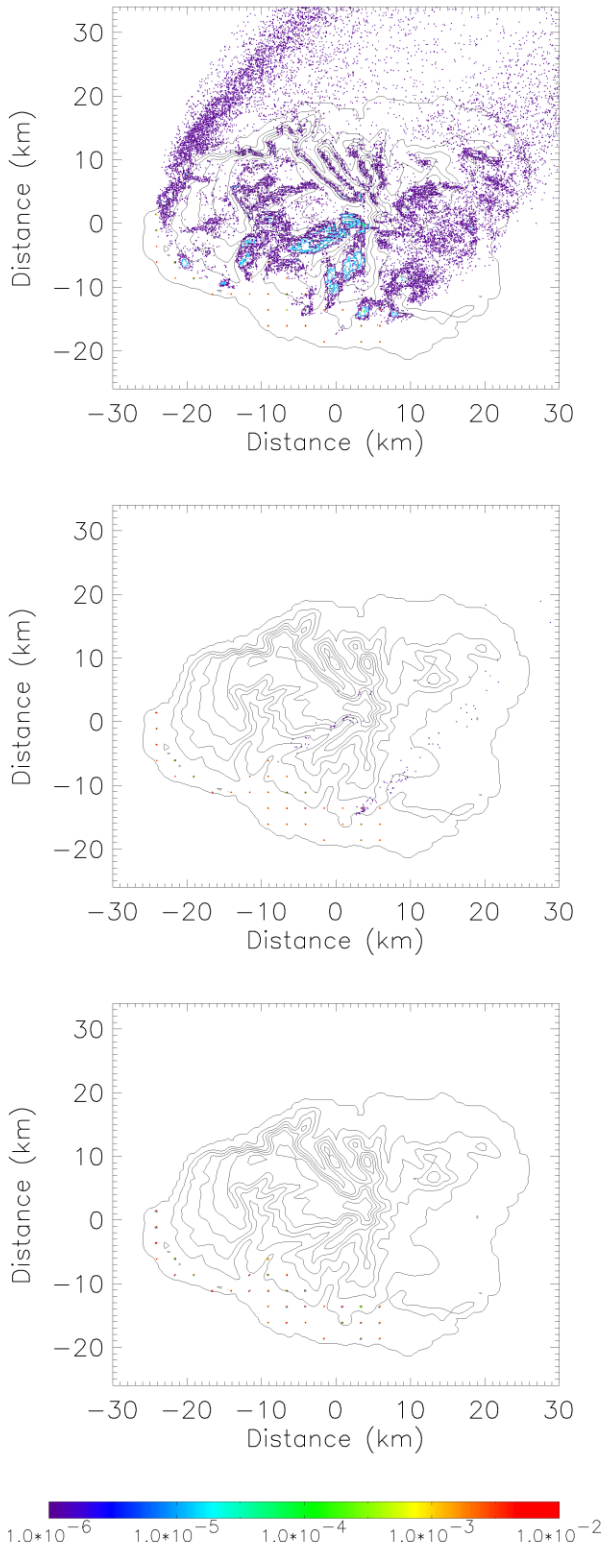
Distance (km)
Distance (km)
30
20
10
0
−10
−20
−30
1.0*10−6
1.0*10−5
1.0*10−4
1.0*10−3
1.0*10−2

Figure 5

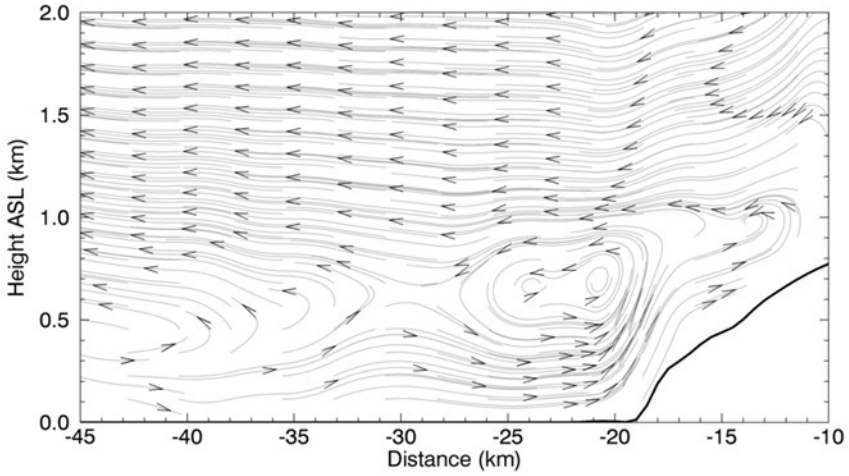

Figure 6

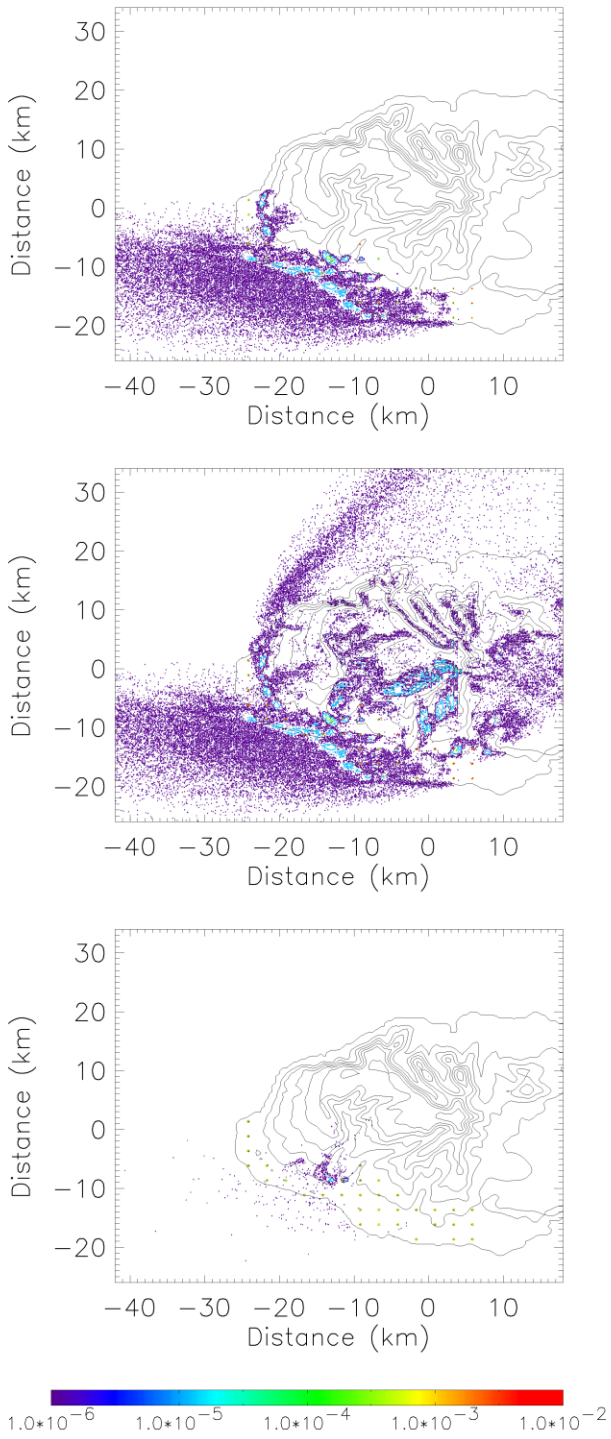
30
20
10
0
−10
−20
Distance (km)
−40 −30 −20 −10 0 10
Distance (km)
1.0∗10−6
1.0∗10−5
1.0∗10−4
1.0∗10−3
1.0∗10−2

1

2 Figure 7

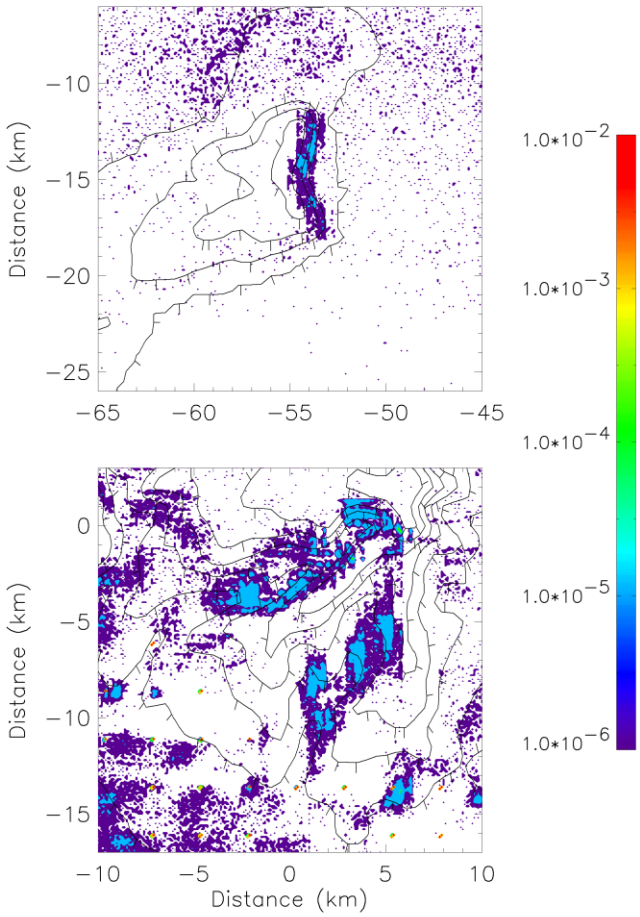
−10
−15
−20
−25
Distance (km)
−65
−60
−55
−50
−45
0
−5
−10
−15
Distance (km)
−10
−5
0
5
10
Distance (km)
1.0*10−2
1.0*10−3
1.0*10−4
1.0*10−5
1.0*10−6

1

2 Figure 8

3

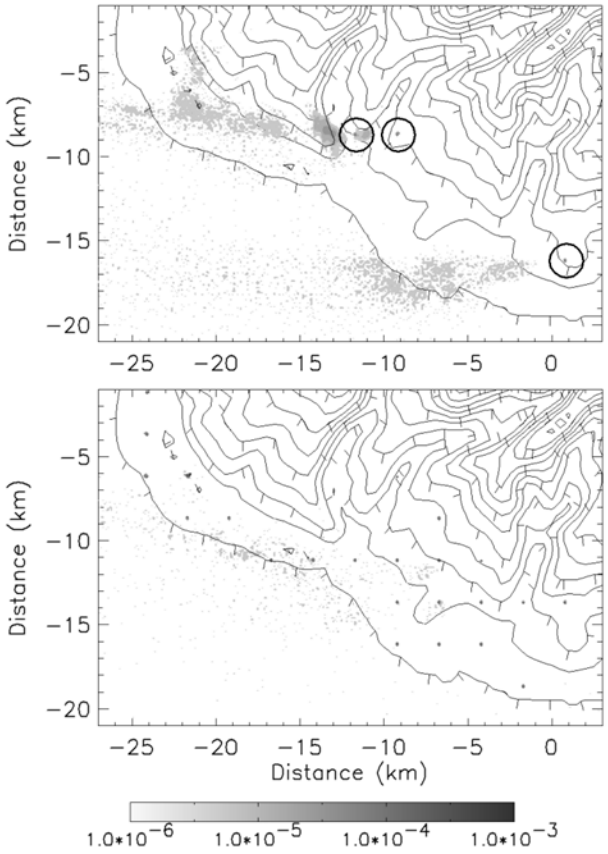
Distance (km)
−5
−10
−15
−20
−25
−20
−15
−10
−5
0
Distance (km)
1.0*10−6
1.0*10−5
1.0*10−4
1.0*10−3

Figure 9

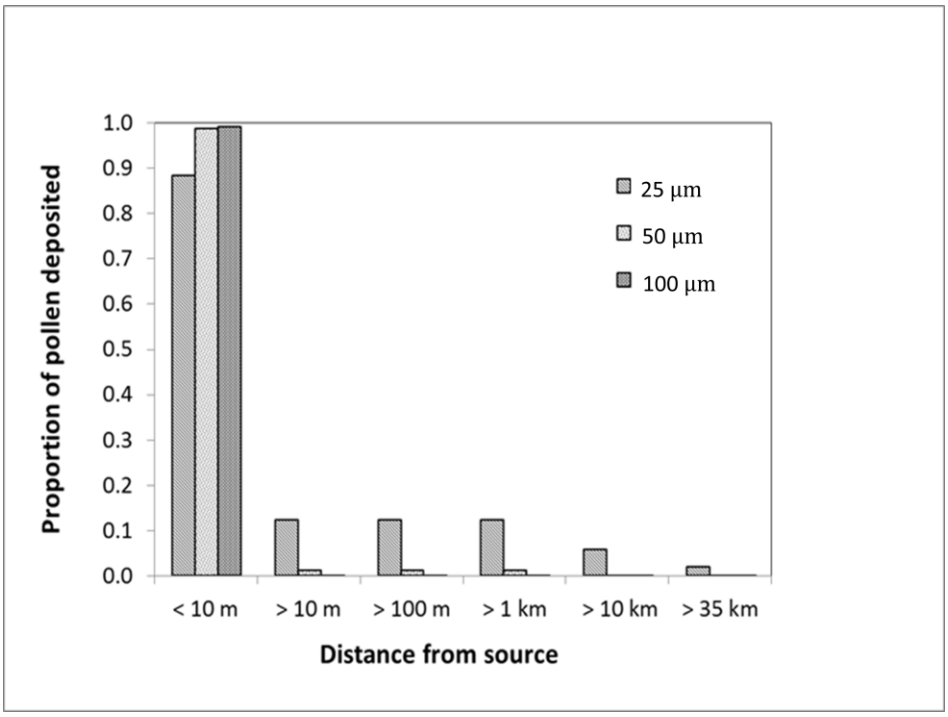
Proportion of pollen deposited
1.0
0.9
0.8
0.7
0.6
0.5
0.4
0.3
0.2
0.1
0.0
25 μm
50 μm
100 μm
< 10 m
> 10 m
> 100 m
> 1 km
> 10 km
> 35 km
Distance from source

Figure 10